

Submitted: September 5, 2022


Revised: September 29, 2022

Accepted: November 23, 2023

Numerical estimation of fatigue life of aluminum alloy specimen with surface defects based on stress-life approach

L.A. Almazova,  O.S. Sedova , 

St. Petersburg State University, St. Petersburg, Russia

 olya-sedova@mail.ru

ABSTRACT

This paper presents a numerical study for fatigue life estimation of a cylindrical specimen made of aluminum alloy under high cycle fatigue regime. The fatigue life is assessed through the stress-life approach. The sample is weakened by either a cluster of surface defects or by an equivalent defect. Two different forms of defects are considered. The load conditions are assumed to be uniaxial tension-compression with a load ratio $R = 0.1$. To account for non-zero mean stress the Goodman correction is used. The material properties are considered to be combined nonlinear isotropic and kinematic hardening implemented in ANSYS Workbench software.

KEYWORDS

aluminum alloy • finite element analysis • FEM • stress-strain state • corrosion pit • fatigue life • surface defect • interaction of defects • cyclic loads

Acknowledgements. This work was supported by Russian science foundation (RSF #21-19-00100).

Citation: Almazova LA, Sedova OS. Numerical estimation of fatigue life of aluminum alloy specimen with surface defects based on stress-life approach. *Materials Physics and Mechanics*. 2024;52(1): 69–80.

http://dx.doi.org/10.18149/MPM.5212024_7

Introduction

Most of the metal structures are subjected to cyclic mechanical loads during their service life. Even if the applied loads never exceed the elastic limit of the material, it is possible that after a certain number of cycles failure may occur. Therefore, it is important to understand how the mechanical properties of the material degrade as a result of the gradual accumulation of damage under the influence of various stresses below the elastic limit, i.e., the fatigue life of the material.

For a correct estimation of fatigue life, it is necessary to determine the appropriate parameters of the metal in question as a result of many experiments, as well as to account for a lot of different factors affecting fatigue behavior such as surface condition, type of loading, environment conditions, etc. The literature analysis indicates that fatigue performance of structures is hard to predict since it depends on numerous parameters.

Moreover, the majority of structures always contain a certain number of defects, which, becoming stress concentrators, reduce the strength and fatigue life of the structure. For metals such local stress concentrators may often result from manufacturing process [1,2] or be induced by corrosion [3–5]. The effect of defects on fatigue strength has been widely studied for decades, nevertheless, a lot of dependencies are still unclear. It is known with reasonable accuracy about two parameters that influence fatigue limit significantly. The first of them is defect size; it was shown by many researchers that fatigue limit decreases with increasing defect size, e.g., [6–9]. The second known

characteristic is defect location: surface, subsurface or internal. Studies, comparing surface and internal defects, clearly showed that surface ones are more dangerous than internal ones, e.g., [6,10,11]. Papers, where subsurface defects were considered, showed that this type of defect location is most harmful to fatigue life [12,13]. Recent experimental research by Nadot [14] performed for different materials and various parameters shows that the defect's size, type and position are among the major parameters affecting fatigue performance. The author notes that assessing fatigue limit in the presence of a defect is indeed a challenging task where many questions are not yet answered. Including those issues of interest named the local material behaviour near defects, which may be not only elastic but also plastic, which is considered in limited research on structures weakened by defects.

The influence of single defects on the stress-strained state of structures has been studied extensively both for surface and internal defects. However, it is obvious that real materials may contain several defects, which, being in close proximity, begin to interact with each other. In particular, defects caused by production activities, namely casting defects or welding defects, corrosion pits, surface roughness, micro inclusions, dislocations, are often located close together, which leads to interaction of fields of stresses and significantly reduces the strength limit of the material [6,15].

In [3,16,17] it is noted that corrosion pits on the surface of steels and aluminum alloys have a complex shape, where the main and secondary pitting at the bottom can be conditionally distinguished. Studies carried out on the modelling of stress-deformed structures containing one corrosion defect of such a complex shape show that the influence of the additional pitting leads to a significant increase in the stress concentration coefficient [16–18].

It is worth mentioning that in situations where the defects are located in close proximity to each other, it is very difficult to determine the actual size and form of damage [11,19]. That is why research designed to find simplified forms that could approximate such complex forms of defects or sets of defects is extremely relevant. Such simplified forms are utilized in a few papers for a variety of problems, where they are usually called “equivalent” forms for the considered complex-shaped surface or internal defects or “equivalent” defects, e.g. [11,20,21].

In [22] a cluster of surface defects is approximated by a rectangle to determine the ultimate strength of a plate with randomly distributed defects. More complex approach which may be considered as multiple equivalent rectangles is used in [23]. Simplified conical, cylindrical and spherical shapes of pits are used [24] to numerically assess the ultimate strength of hull structural plate with multiple local corrosion defects. Rounded rectangles are also utilized to approximate complex-form defects or set of defects [21,25,26]. Note that in papers [21,25,26], where the defects are simplified by rounded rectangles, the rounded edge serves for avoiding singularities in finite element analysis, yet the possible effect of the different values of the rounding radius is not studied. Authors of [24,27,28] showed that the form of defects (circular, conical, elliptical or cylindrical) has a slight effect on strength of plates under different loading. However, in the mentioned papers neither the effect of varying sizes of the defect with rounded rectangle form nor the influence of complex forms of defects are not considered.

Experimental and numerical research for aluminum alloy under cyclic load is conducted in [20]. Spherical and three types of complex form artificial defects were introduced in specimens. Fatigue test results were complemented by finite element analysis conducted for geometries with two types of equivalent defect forms: spherical and elliptical. Simulations performed with elliptical defects provided better correspondence with experimental results. The possible reason for that might be that the elliptical defects account for the orientation of the defect which is extremely important for fatigue life prediction.

The impact of surface defect interaction is investigated in order to assess the high cycle fatigue performance of aluminum alloy in [21]. Nonlinear hardening is used to describe the material behaviour under uniaxial cyclic load. The stress distribution around the cluster of three hemispherical defects on the surface of a cylindrical specimen is numerically calculated. Circumferential and longitudinal configurations of defects are considered as well as various defect sizes, distances between defects and applied loads. The numerical results obtained through the Crossland criterion are compared with experiments by Mu et. al. [29]. Additionally, authors [21] proposed substituting three interacting hemispherical surface defects with a single equivalent defect in the shape of a rounded rectangle. The calculated fatigue limit of the model with the equivalent defect is compared with the fatigue limit of the model with three interacting defects. It is concluded that the fatigue limit of specimens with the cluster of defects can be estimated by the finite analysis of the model with the single equivalent defect. The authors report that the fatigue limit obtained using the equivalent defect is greater than with three interacting hemispherical defects, with the difference being within 7%. However, it remains unexplored whether the equivalent defect sizes proposed in [21] are optimal, and whether the suggested method can be applied to estimate the fatigue limit when defects are of complex forms [3,16,17]. These questions are addressed in the present paper.

In this paper, the fatigue life of a specimen made of aluminum alloy is assessed. Fatigue life is determined by the SN curve method. The specimen is weakened by a cluster of surface defects. Three hemispherical defects and three defects of a complex shape, where the main and secondary hemispherical pitting at the bottom can be conditionally distinguished, are considered. The defects are located in close proximity to each other so that the interaction of stress fields takes place. Three models with corresponding equivalent defects that could approximate complex forms of the considered sets of defects are constructed and analyzed. The combined nonlinear isotropic and kinematic hardening model is utilized to describe the material behaviour. The mean stress correction is used to account for the effect of non-zero mean stresses.

Fatigue life assessment

The most common approaches for assessing fatigue damage under cyclic loading are a stress-life approach, a strain-life approach and fracture mechanics approach [30]. In stress-life and strain-life approaches, the number of cycles to failure is represented as a function of alternating stress and mean stress, alternating stress and R-ratio (defined as a ratio of the minimum stress value to the maximum stress value), and alternating strain and mean strain, respectively [30]. In fracture mechanics approach the rates of growing cracks are analyzed to assess fatigue life [30].

The stress–life approach is used in applications where the applied stress is essentially within the elastic range, and the material has a long cyclic life. This approach is suitable when the degree of plastic straining is negligible, as in high cycle fatigue regime (HCF), where plastic strains are relatively small and concentrated in a small area. Stress–life data is usually represented by SN curve, which is either plotted as a log-linear or a log-log plot. SN curve is obtained from constant-amplitude uniaxial cyclic tests performed for a given material for different alternating stresses with the same stress ratio R . Different SN curves are therefore generated for different R -ratios. The Basquin model is widely used to determine fatigue life in terms of stress–life in the case of uniaxial loads for multi-cycle fatigue [31]. According to this model based on fatigue curves, the difference between the minimum and maximum stresses in the cycle is linearly related to the number of cycles before the destruction [32]:

$$\sigma_a N_f^b = c, \quad (1)$$

where N_f is the number of cycles before destruction, σ_a – stress amplitude of a symmetric loading cycle, $b = \text{const}$ – fatigue strength exponent, $c = \text{const}$. For the cases where mean stress is non-zero, the load amplitude needs to be corrected before using Eq. (1). The parameters b and c depend on the material properties. Numerical parameters of the Basquin model are determined by the SN curve of the alloy considered.

The strain–life approach considers the plastic deformation that may occur during fatigue loading. This method accounts for localized yielding, which is often the case in metal components corresponding to low cycle fatigue (that is a relatively short fatigue life, usually less than 10^5 cycles). In such a case, the plastic deformation of a material may take place not only in a small area near stress concentrators.

In this research, fatigue life is assessed through the stress-life approach using Basquin's relation Eq. (1).

Mean stress correction

SN curve methods are widely used to estimate fatigue life of materials under symmetrical loading conditions, i.e., where mean stress is zero. As mentioned above, by performing multiple tests it is possible to obtain the SN curves for a considered material under different mean stress conditions. It is obvious that resources for conducting experiments are quite limited, or it may be impossible to create the necessary conditions. Thus, the case with a zero mean stress has become the one that has been most studied experimentally. Whereas, when the magnitude of loading in both directions is different, mean stress value plays a vital role in fatigue life estimation [33–35]. Non-zero mean stress may decrease or increase the estimated life depending on parameters of a problem [35]. There are variety of models for the mean stress correction developed for different materials and conditions, e.g. [36–38]. Such models allow one to use the data from experiments with zero mean stress for a case where the mean stress is non-zero. The mean stress correction essentially provides the stress amplitude called equivalent amplitude (with zero mean stress) which results in the same fatigue damage as the given non-symmetric stress amplitude (with non-zero mean stress). By means of equivalent amplitude fatigue life is assessed. Some of the common mean stress correction methods are the Coffin–Manson relationship [39], Morrow's mean stress approach [40] and the

Smith, Watson and Topper [41]. A new model to account for the mean stress is proposed and found to be valid for different materials in [42].

One of the widely used mean stress corrections is Goodman equation [43] that is generally suitable for brittle materials [44]:

$$\frac{\sigma_a}{\sigma_{ar}} + \frac{\sigma_m}{\sigma_u} = 1, \quad (2)$$

where σ_a – is the stress amplitude, σ_m – mean stress, σ_u – ultimate tensile strength. That used to solve for σ_{ar} – equivalent amplitude of a corresponding symmetric cycle.

Smith-Watson-Topper (SWT) mean stress correction is a good choice for general use and quite accurate for aluminum alloys [41,45,46]:

$$\sigma_{ar} = \sigma_{max} \sqrt{\frac{1-R}{2}}, \quad (3)$$

where $\sigma_{max} = \sigma_m + \sigma_a$.

Problem formulation

The cylindrical sample of aluminum alloy either with a cluster of three corrosion defects or with a single equivalent defect is considered under HCF regime. The load conditions are assumed to be uniaxial tension-compression with $R = 0.1$. The problem is to numerically assess the fatigue life of a sample for various load values and different defect shapes. Mean stress correction is made by Goodman theory (Eq. (2)). The distribution of von Mises stress under static uniaxial tension is also analyzed.

Material

The paper considers the alloy AS7G06 with T6 post-thermal treatment. The chemical composition are shown in the Table 1 [29].

Table 1. Chemical composition of AS7G06

Element	Si	Mg	Fe	Cu	Mn	Ni	Zn	Pb	Ti
%	7.00	0.56	0.097	<0.015	<0.03	<0.01	<0.01	<0.003	0.13

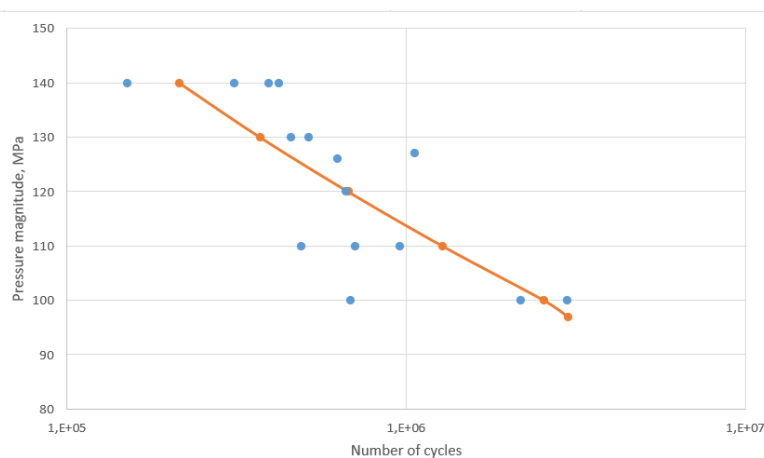


Fig. 1. SN curve for AS7G06: blue dots correspond to experimental results [29], orange curve results from fitting a set of data points with a quadratic function

The material parameters are specified in the ANSYS Workbench package in the Engineering Data section. The material behavior is described by a model with a combined nonlinear isotropic and kinematic hardening implemented in ANSYS Workbench.

Moreover, SN curve for the considered material (Fig. 1) obtained in [29] was used to find numerical parameters needed for fatigue life estimation.

Model

The geometric model was built in the ANSYS SpaceClaim package. The elementary model in question is a cylinder corresponding to the gauge part of the experimental samples either with a cluster of surface defects or with a single equivalent defect. Cylinder has a diameter 10 mm and length 20 mm. Five geometries with differently shaped defects have been constructed:

1. A sample with three hemispherical defects (Fig. 2(a)). All hemispherical defects are equal to each other, their radii are set to $r_m = 0.32$ mm. The distance between defects equals 0.1 mm.
2. A sample with three defects of a complex form: every defect consists of the main defect and a secondary damage at the bottom of the main one (Fig. 2(b)). Both the main and secondary damage are of a hemispherical form. All main defects are equal to each other, their radii are set to $r_m = 0.32$ mm. The distance between main defects equals 0.1 mm. All secondary defects are equal to each other and have a radius $r_s = 0.08$ mm.
3. A sample with one equivalent defect to approximate geometry (i). The defect is modeled as a rectangle cut with a rounded edge. The rectangle dimensions are length = $6r_m$, width = $2r_m$ and height = $\frac{r_m}{2}$, the radius of curvature of a rounded edge is $0.1r_m$.
4. A sample with one equivalent defect to approximate geometry (i) (Fig. 2(c)). The defect is modeled as a rectangle cut with a rounded edge. The rectangle dimensions are length = $6r_m$, width = $2r_m$ and height = $\frac{r_m}{4}$, the radius of curvature of a rounded edge is $0.1r_m$.
5. A sample with one equivalent defect to approximate geometry (ii) (Fig. 2(d)). The defect is modeled as a rectangle cut with a rounded edge. The rectangle dimensions are length = $6r_m$, width = $2r_m$ and height = $r_m + r_s$, the radius of curvature of a rounded edge is $0.1r_m$.

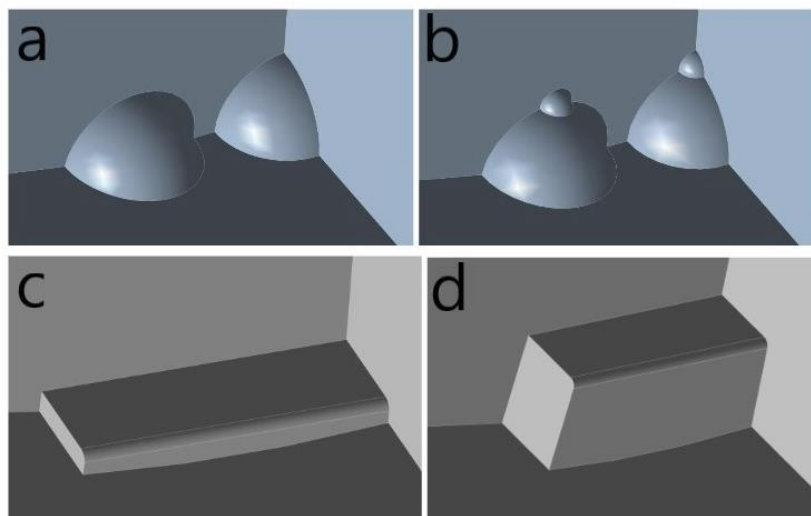


Fig. 2. Geometries with differently shaped defects

Due to symmetry, only a one fourth part of each of the considered models was constructed (see Fig. 3). It should be noted that sizes in geometry descriptions (i–v) are given for the whole elementary models. Consequently, in constructed parts with the equivalent defect (iii –v), the length and width of the defect are $3r_m$ and r_m , respectively. The height of the equivalent defect in one fourth part of each of the considered models (iii –v) remains as indicated above.

The constructed geometric models have the following boundary conditions: on the cross-section corresponding to the boundary of the gauge part of the sample, the force corresponding to the amplitude in cyclic tests is applied; the symmetry condition (“frictionless support” condition in ANSYS Workbench) acts on the cross-section planes of the quarter of the model (planes a and b in Fig. 3).

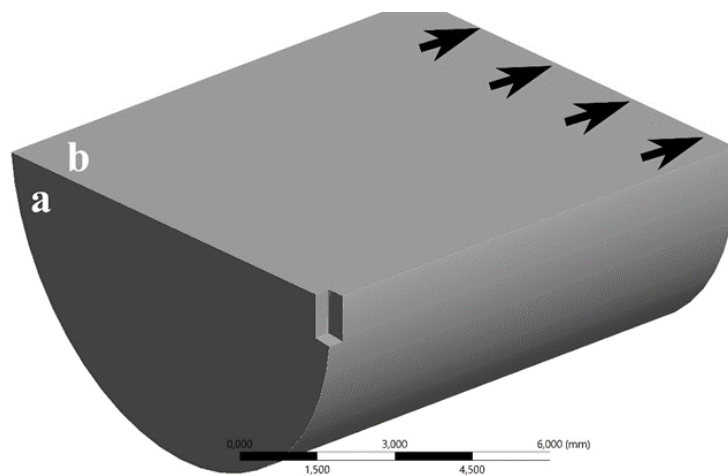


Fig. 3. A geometrical model with the equivalent-form defect: a, b – the planes with symmetry condition; arrows indicate the plane of load application and direction

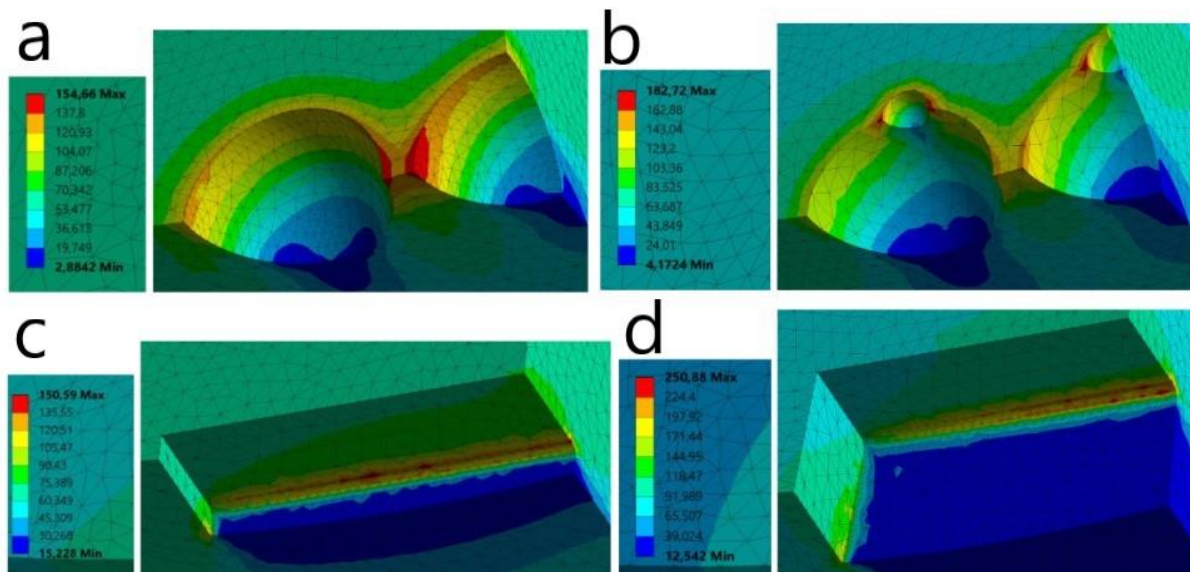


Fig. 4. Stress distribution for constructed geometries (stress values are given in MPa)

To use the finite element method, a tetrahedron mesh was constructed. Moreover, since the vicinity of the defects is a probable place of stress concentration, the face sizing method was additionally applied to the surface of the defects, allowing to set a fine grid in the specified areas (Fig. 4).

The mesh convergence study was carried out in order to ensure the accuracy of solution. With various finite element meshes, several static analysis simulations for geometry with three surface defects of a complex form (geometry (ii)) were conducted. Figure 5 shows the maximum von Mises stress corresponding to the number of elements in a certain mesh. It was found that for meshes with the number of elements over 10^6 the relative differences between results of considered simulations is less than 4 %. Therefore, for further analysis the number of elements was approximately 1.2×10^6 .

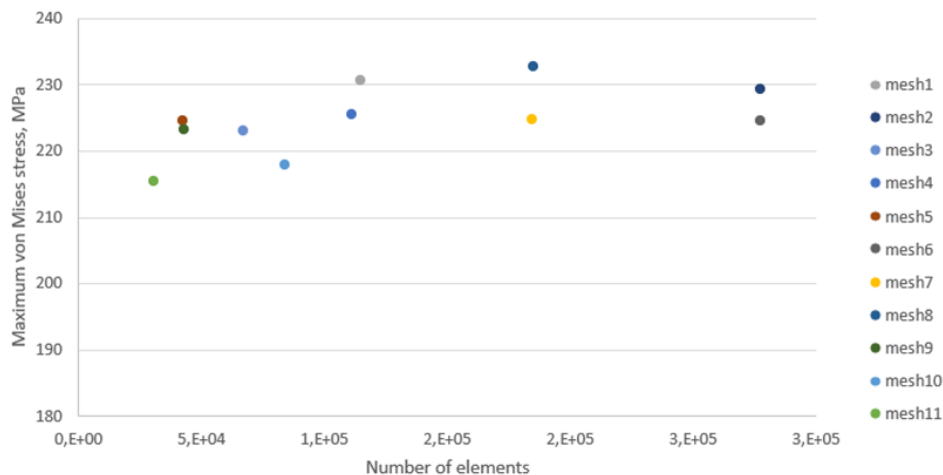


Fig. 5. Mesh convergence of maximum von Mises stress obtained with different meshes

Results

Stress distributions near the local defects for the set of geometries in question are presented in Fig. 4 for the applied static load equal to 60 MPa. They clearly demonstrate that for geometries with a cluster of three pits (i) and (ii) (Fig. 4(a,b), respectively) a significant increase in the value of the von Mises stress is observed in the presence of the secondary damage (geometry (ii), Fig. 4(b)). Note that in the case of defects of a complex shape (Fig. 4(b)), the maximum stress values are reached at the joint of the secondary defects with the main ones. For geometry (i) with three defects of a hemispherical form (without a secondary damage), the maximum of the von Mises stress is achieved at the sharp edges between the defects (Fig. 4(a)). This result is in accordance with [21,48,49].

From Fig. 4 it is seen that the difference between maximum stress values in a sample with three hemispherical pits (i, Fig. 4(a)) and a sample with equivalent defect (iv, Fig. 4(c)) is below 3 %. While the difference between values of maximum stress obtained in geometry (ii, Fig. 4(b)) with a cluster of complex-shaped pits and the geometry (v, Fig. 4(d)) with the equivalent defect is over 30 % for a considered load. Therefore, the equivalent defect (iv) provides a good approximation of a cluster of hemispherical pits (i) in terms of prediction of stress values for static analysis (Figs. 4(a,c)). At the same time, none of the considered equivalent defects (iii–v) allows to estimate the stress values near

a cluster of complex-shaped pits (ii) for static analysis. It should be noted that the difference between results obtained for a sample with three hemispherical pits (i, Fig. 4(a)) and for the equivalent defect (iii) is sufficiently more than 3 %.

The dependencies of calculated fatigue life values of constructed models (i–v) from values of applied loads at $R = 0.1$ with the Goodman mean stress correction (Eq. (2)) are shown in Fig. 6. It can be seen that the maximum life of geometries considered coincides, but in the case of defects of a complex shape (geometry (ii), solid orange curve) it is achieved at a maximum load of 60 MPa, while for geometry with defects of a hemispherical form without a secondary damage (geometry (i), solid blue curve) the maximum value of fatigue life is maintained up to a load of 90 MPa. In this case, the maximum load at which a structure with secondary damages (geometry (ii)) does not undergo instantaneous destruction reaches 60 MPa when for the second model (geometry (i)), it reaches 90 MPa. Thus, the presence of a secondary defect at the bottom of the main one causes a significant decrease in strength. Note that in contrast to steel and titanium alloys, aluminum alloys do not have a distinct fatigue limit. Consequently, aluminum specimens are susceptible to fatigue failure, even under minimal stress amplitudes.

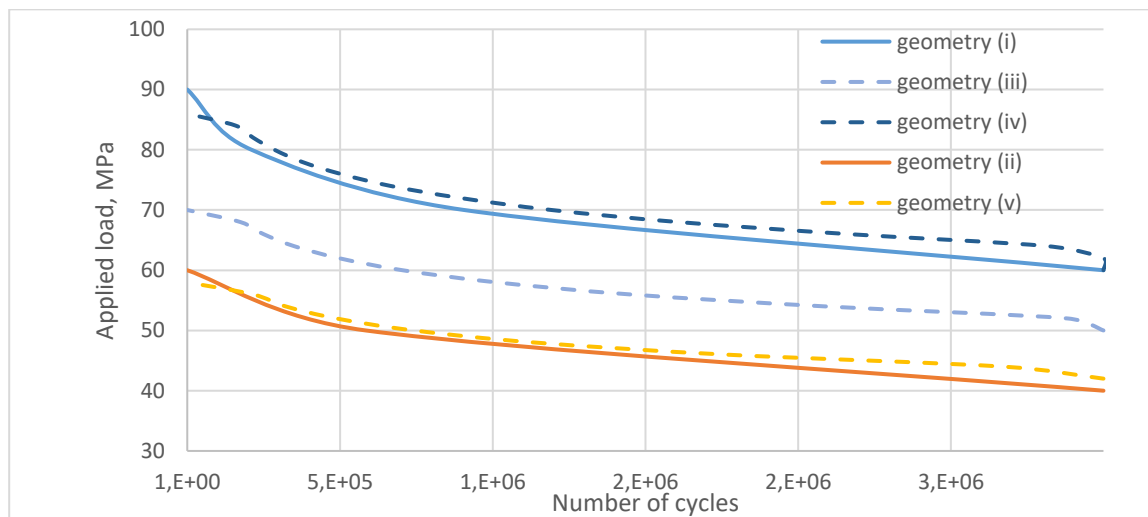


Fig. 6. Dependence of fatigue life from values of applied loads

It is seen from Fig. 6 that the curves for geometries (i) and (iv), (ii) and (v) are close to each other for all considered applied loads. However, the analysis of results showed that for a fixed load value the estimated lifetimes between geometries (i) and (iv) may reach 40 %. This difference grows with the growing applied load. For loads under 66 MPa the difference is less than 30 %. In the same way the difference between the estimated fatigue lifetimes between geometries (ii) and (v) grows as load grows, reaching 33 % at 56 MPa. For loads under 48 MPa the difference is less than 26%.

Thus, the geometries with equivalent defects (iv) and (v) provide overestimated values of calculated fatigue lifetimes up to 40 and 33 %, respectively, compared with the results of lifetimes obtained using geometries with pit clusters (i) and (ii).

Conclusions

In the paper a cylindrical sample of aluminum alloy either with a cluster of surface defects or with a single equivalent defect is considered at high cycle fatigue regime under uniaxial tension-compression load with ratio $R = 0.1$. Using ANSYS Workbench the fatigue life of a sample for various load values and different defect shapes is numerically assessed. Goodman mean stress correction is performed to account for non-zero mean stress. The distribution of von Mises stress under static uniaxial tension is also analyzed for different defect shapes.

It was found that the equivalent defect may be used for prediction of stress values for a specimen with a cluster of three hemispherical pits for static analysis.

It was shown that the form of surface pits plays significant role for the calculated fatigue life. Complex form of surface defects reduces fatigue strength.

The error of modelling a cluster of three pits by a single equivalent defect grows with the growing applied load for both considered shapes of pits. The assessment of fatigue life of locally corroded specimens through a single equivalent defect may provide overestimated values of fatigue lifetimes up to 40 % for a cluster of three hemispherical pits and up to 33 % for a cluster of three complex-shaped pits.

References

1. Wang QG, Crepeau PN, Davidson CJ, Griffiths JR. Oxide films, pores and the fatigue lives of cast aluminum alloys. *Metallurgical and Materials Transactions*. 2006;37(B): 887–895.
2. Biswal R, Zhang X, Syed AK, Awd M, Ding J, Walther F, Williams S. Criticality of porosity defects on the fatigue performance of wire + arc additive manufactured titanium alloy. *International Journal of Fatigue*. 2019;122: 208–217.
3. Genel K, Demirkol M, Gülmez T. Corrosion fatigue behaviour of ion nitrided AISI 4140 steel. *Materials Science and Engineering*. 2000;288(1): 91–100.
4. Co NEC, Burns JT. Effects of micro-scale corrosion damage features and local microstructure on fatigue crack initiation location. *International Journal of Fatigue*. 2021;150: 106301.
5. Fabas A, Monceau D, Doublet S, Put AR. Modelling of the kinetics of pitting corrosion by metal dusting. *Corros. Sci.* 2015;98: 592–604.
6. Murakami Y. *Metal Fatigue: Effects of Small Defects and Nonmetallic Inclusions*. Chennai. Academic Press. 2019.
7. Wang ML, Yang XG, Li B, Shi DQ, Miao GL, Guo SQ, Fan YS. The dominant role of defects on fatigue behaviour of a SLM Ni-based superalloy at elevated temperature. *International Journal of Fatigue*. 2023;176: 107894.
8. Yang L, Cai P, Xu Z, Jin Y, Liang C, Yin F, Zhai T. A 3-D model for quantification of fatigue weak-link density and strength distribution in an A713 cast aluminum alloy. *International Journal of Fatigue*. 2017;96: 185–195.
9. Wu X, Schlangen E, van der Zwaag S. Linking porosity to rolling reduction and fatigue lifetime of hot rolled AA7xxx alloys by 3D X-ray computed tomography. *Adv. Eng. Mat.* 2012;14(7): 457–463.
10. Serrano-Munoz I, Buffiere JY, Verdu C, Gaillard Y, Mu P, Nadot Y. Influence of surface and internal casting defects on the fatigue behaviour of A357-T6 cast aluminium alloy. *International Journal of Fatigue*. 2016;82: 361–370.
11. Yamashita Y, Murakami T, Mihara R, Okada M, Murakami Y. Defect analysis and fatigue design basis for Ni-based Superalloy 718 manufactured by selective laser melting. *International Journal of Fatigue*. 2018;117: 485–495.
12. Pineau A, Antolovich S. D. Probabilistic approaches to fatigue with special emphasis on initiation from inclusions. *International Journal of Fatigue*. 2016;93: 422–434.
13. Fan J, McDowell DL, Horstemeyer MF, Gall K. Cyclic plasticity at pores and inclusions in cast Al–Si alloys. *Engineering Fracture Mechanics*. 2003;70(10): 1281–1302.
14. Nadot Y. Fatigue from Defect: Influence of Size, Type, Position, Morphology and Loading. *International Journal of Fatigue*. 2022;154: 106531.
15. Leitner M, Murakami Y, Farajian M, Remes H, Stoschka M. Fatigue Strength Assessment of Welded Mild Steel Joints Containing Bulk Imperfections. *Metals*. 2018;8(5): 306.

16. Cerit M, Genel K, Eksi S. Numerical investigation on stress concentration of corrosion pit. *Engineering Failure Analysis*. 2009;16(7): 2467–2472.
17. Zhao W, Huang YF, Ye XB, Hu BR, Liu JZ, Chen LJ. Correlation between the Geometric Parameters of Corrosion Pit and Stress Concentration Factor. *Applied Mechanics and Materials*. 2013;327: 156–160.
18. Cerit M. Corrosion pit-induced stress concentration in spherical pressure vessel. *Thin-Walled Structures*. 2019;136:106–112.
19. Beretta S, Romano S. A comparison of fatigue strength sensitivity to defects for materials manufactured by AM or traditional processes. *International Journal of Fatigue*. 2017;94: 178–191.
20. Rotella A, Nadot Y, Piellard M, Augustin R, Fleuriot M. Influence of defect morphology and position on the fatigue limit of cast Al alloy: 3D characterization by X-ray microtomography of natural and artificial defects. *Materials Science and Engineering: A*. 2020;785: 139347.
21. Ben Ahmed A, Nasr A, Bahloul A, Fathallah R. The impact of defect morphology, defect size, and SDAS on the HCF response of A356-T6 alloy. *The International Journal of Advanced Manufacturing Technology*. 2017;92(1): 1113–1125.
22. Ok D, Pu Y, Incecik A. Computation of ultimate strength of locally corroded unstiffened plates under uniaxial compression. *Marine Structures*. 2007;20(1–2): 100–114.
23. Khedmati MR, Nouri ZHME. Analytical simulation of nonlinear elastic–plastic average stress–average strain relationships for un-corroded/both-sides randomly corroded steel plates under uniaxial compression. *Thin-Walled Structures*. 2015;86: 132–141.
24. Zhang Y, Huang Y, Zhang Q. Ultimate strength of hull structural plate with pitting corrosion damage under combined loading. *Ocean Engineering*. 2016;116: 273–285.
25. Tee KF, Wordu AH. Burst strength analysis of pressurized steel pipelines with corrosion and gouge defects. *Eng. Fail. Anal.* 2020;108: 104347.
26. Gao J, Yang P, Li X, Zhou J, Liu J. Analytical prediction of failure pressure for pipeline with long corrosion defect. *Ocean Eng.* 2019;191: 106497.
27. Zhao Z, Zhang H, Xian L, Liu H. Tensile strength of Q345 steel with random pitting corrosion based on numerical analysis. *Thin Wall. Struct.* 2020;148: 106579.
28. Huang Y, Zhang Y, Liu G, Zhang Q. Ultimate strength assessment of hull structural plate with pitting corrosion damage under biaxial compression. *Ocean Eng.* 2010;37(17–18): 1503–1512.
29. Mu P, Nadot Y, Serrano-Munoz I, Chabod A. Influence of complex defect on cast AS7G06-T6 under multiaxial fatigue loading. *Engineering Fracture Mechanics*. 2014;123: 148–162.
30. Dowling NE. A Review of Fatigue life Prediction Methods. *SAE International*. 1987;96(3): 1117–1138.
31. Bonnand V, Chaboche JL, Cherouali H, Kanoute P, Ostojica-Kuczynski E, Vogel F. Investigation of multiaxial fatigue in the prospect of turbine disc applications: Part II, Fatigue criteria analysis and formulation of a new combined one. In: *Proc. 9th Int. Conf. of Multiaxial Fatigue and Fracture (ICMFF9)*. Parma, Italy; 2010. p.691–698.
32. Schijve J. (eds.) *Fatigue of Structures and Materials*. Dordrecht: Springer; 2009.
33. Kumbhar SV, Tayade RM. A case study on effect of mean stress on fatigue life. *International Journal of Engineering Development and Research*. 2014;2(1): 304–308.
34. Bader Q, Kadum E. Mean stress correction effects on the fatigue life behavior of steel alloys by using stress life approach theories. *Int. J. Eng. Technol.* 2014;10: 50.
35. Böhm M, Kluger K, Pochwała S, Kupina M. Application of the SN curve mean stress correction model in terms of fatigue life estimation for random torsional loading for selected aluminum alloys. *Materials*. 2020;13(13): 2985.
36. Dowling NE. Mean stress effects in stress-life and strain-life fatigue. *SAE International*. 2004;32(12): 1004–1019.
37. Ince A. A mean stress correction model for tensile and compressive mean stress fatigue loadings. *Fatigue & Fracture of Engineering Materials & Structures*. 2017;40(6): 939–948.
38. Zhu SP, Lei Q, Huang HZ, Yang YJ, Peng W. Mean stress effect correction in strain energy-based fatigue life prediction of metals. *International Journal of Damage Mechanics*. 2017;26(8): 1219–1241.
39. Manson SS, Halford GR. Practical implementation of the double linear damage rule and damage curve approach for treating cumulative fatigue damage. *International Journal of Fracture*. 1981;17(2): 169–192.
40. Morrow J. Fatigue properties of metals. In: *Section 3.2, Fatigue Design Handbook*. Society of Automotive Engineers. 1968; AE-4.
41. Ince A, Glinka G. A modification of Morrow and Smith–Watson–Topper mean stress correction models. *Fatigue Fracture Engineering Material Structure*. 2011;34(1) 854–867.
42. Liu Y, Paggi M, Gong B, Deng C. A unified mean stress correction model for fatigue thresholds prediction of metals. *Engineering Fracture Mechanics*. 2020;223: 106787.
43. Goodman J. *Mechanics applied to engineering*. Longmans, Green; 1919.
44. Smith JO. The Effect of Range of Stress on the Fatigue Strength of Metals. *Bulletin*. 1942;334: 7–47.

45. Smith KN, Watson P, Topper TH. A Stress-Strain Function for the Fatigue of Metals. *Journal of Materials*. 1970;5(4):767–778.
46. Papuga J, Vízková I, Lutovinov M, Nesládek M. Mean stress effect in stress-life fatigue prediction re-evaluated. *MATEC Web Conf*. 2018;165: 10018.
47. Sun J, Cheng YF. Modeling of mechano-electrochemical interaction between circumferentially aligned corrosion defects on pipeline under axial tensile stresses. *J. Petrol. Sci. Eng*. 2021;198: 108160.
48. Liao Y, Liu C, Wang T, Xu T, Zhang J, Ge L. Mechanical behavior analysis of gas pipeline with defects under lateral landslide. *Journal of Mechanical Engineering Science*. 2021;235(23): 6752–6766.
49. Almazova LA, Sedova OS. Simulation of the surface defects influence on the aluminum alloy behaviour under the cyclic load conditions. *Frontier Materials & Technologies*. 2022;1: 7–14. (In Russian)

About Authors

Liana A. Almazova  

Researcher (St. Petersburg State University, St. Petersburg, Russia)

Olga S. Sedova  

Candidate of Physical and Mathematical Sciences

Associate Professor (St. Petersburg State University, St. Petersburg, Russia)